These expressions, which may be useful for numerical calculations, are obtained by using the generating function of the Laguerre polynomials $L_n(x)$:

$$\exp[-x/(1-t)] = (1-t)\exp(-x)\sum_{n=0}^{\infty} t^n L_n(x).$$

Indeed, in (22′), using

$$x_o = \mu s_o/(1-\mu\tau), \quad \tau' = \tau/(1-\mu\tau), \quad q = p_h + \mu,$$

we can write

$$\begin{aligned}\exp[-s_o\mu/(1+\tau p_h)] &= \exp[-x_o/(1+\tau' q)] \\ &= \exp(-x_o)(1+\tau' q)\sum_{n=0}^{\infty}(-\tau' q)^n L_n(x_o) \\ &= \exp(x_o)\left\{1+\sum_{n=0}^{\infty}(-\tau' q)^n[L_n(x_o)-L_{n-1}(x_o)]\right\}.\end{aligned}$$

The formulae (40) are then obtained by using the inverse Laplace transform of $q^n \exp(-s_o\chi^2 E^2/q)$.

References

AL HADDAD, M. & BECKER, P. (1988). *Acta Cryst.* A**44**, 262-270.
BECKER, P. & AL HADDAD, M. (1989). *Acta Cryst.* A**45**, 333-337.
BECKER, P. & AL HADDAD, M. (1990). *Acta Cryst.* A**46**, 123-129.
BECKER, P. & AL HADDAD, M. (1992). *Acta Cryst.* A**48**, 121-134.
BUSHUEV, V. A. (1989). *Sov. Phys. Crystallogr.* **34**, 163-167.
GUIGAY, J. P. (1989). *Acta Cryst.* A**45**, 241-244.
GUIGAY, J. P. (1990). A**46**, C413.
HOLY, V. & GABRIELYAN, K. T. (1987). *Phys. Status Solidi B*, **140**, 39-50.
KATO, N. (1980*a*). *Acta Cryst.* A**36**, 763-769.
KATO, N. (1980*b*). *Acta Cryst.* A**36**, 770-778.
KATO, N. (1991). *Acta Cryst.* A**47**, 1-11.
POLYAKOV, A. M., CHUKHOVSKII, F. N. & PISKUNOV, D. I. (1991). *Sov. Phys. JETP*, **72**, 330-340.

Acta Cryst. (1992). A**48**, 826-829

The Observation of Phonons in Barium Fluoride by Pulsed Neutron Diffraction

BY C. J. CARLILE, D. A. KEEN AND C. C. WILSON

*ISIS Science Division, Rutherford Appleton Laboratory, Chilton, Didcot, Oxfordshire OX*11 0*QX, England*

AND B. T. M. WILLIS

Chemical Crystallography Laboratory, University of Oxford, 9 *Parks Road, Oxford OX*1 3*PD, England*

(*Received* 19 *December* 1991; *accepted* 9 *April* 1992)

Abstract

Measurements of thermal diffuse scattering from a single crystal of barium fluoride made on the neutron time-of-flight Laue single-crystal diffractometer SXD are presented. These measurements are shown to confirm present theories on the nature of the processes producing this scattering effect and their striking variation with scattering geometry.

1. Introduction

In earlier papers (Willis, 1986; Schofield & Willis, 1987), we have discussed the nature of thermal diffuse scattering (TDS) which occurs close to the Bragg reflections in time-of-flight neutron diffraction. Some of the theoretical predictions arising from these studies have received experimental support from observations on pyrolytic graphite (Willis, Carlile, Ward, David & Johnson, 1986) and on single crystals of barium fluoride and calcium fluoride (Carlile & Willis, 1989). These experiments were performed on the high-resolution powder diffractometer (HRPD) at the ISIS Pulsed Neutron Facility, using scattering angles around $2\theta = 174°$. We have now carried out similar experiments with the single-crystal diffractometer (SXD) at ISIS using reduced scattering angles around $2\theta = 90°$ and $2\theta = 125.5°$. Some striking new features occur in the TDS pattern at these lower scattering angles. We shall give an account of these new observations and show that they can also be explained satisfactorily by theory.

2. Time-of-flight study of TDS from barium fluoride

The single-crystal diffractometer SXD at ISIS is a time-of-flight Laue instrument ideally suited to surveying measurements in reciprocal space. The instrument has a short primary flight path ($L_1 = 8$ m, compared with the HRPD with $L_1 \simeq 100$ m). In spite of the poorer resolution of the instrument ($\sim 5\times10^{-3}$ in $\Delta Q/Q$ compared with 5×10^{-4} for HRPD), it is straightforward to observe the TDS features of interest in this work.

0108-7673/92/060826-04$06.00

A schematic diagram of the main components of the SXD is given in Fig. 1. The position-sensitive detector used in the current experiment consisted of an array of 16×16 fibre-optically encoded pixels viewing a lithium-loaded zinc sulfide plastic scintillator. With a pixel resolution of ~ 5 mm and the detector positioned 230 mm from the sample, the resolutions in all three dimensions (time of flight and two spatial directions) are well matched. In the present experiment, the scattering angle for the central element was fixed either at 90 or at 125.5° with the detector array covering a range in scattering angles of ±9.9°.

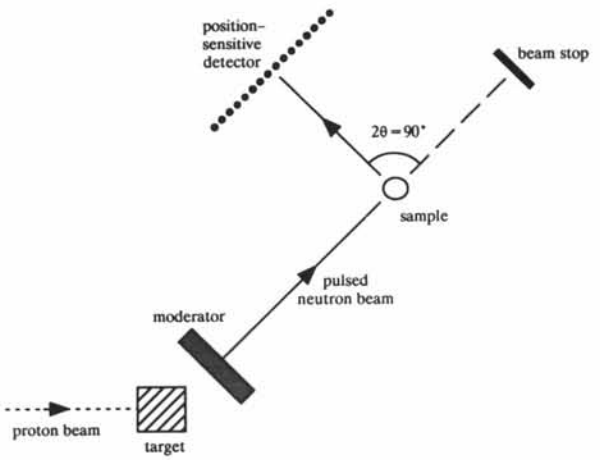

Fig. 1. Schematic diagram showing the layout of the SXD.

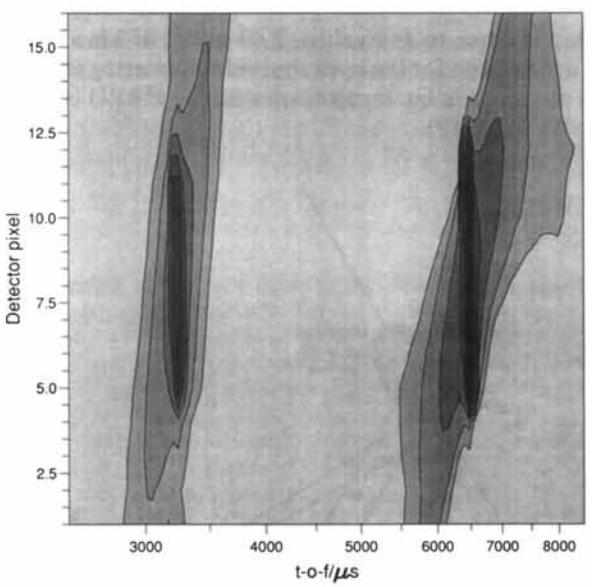

Fig. 2. Contour plot of the 220 and 440 reflections of BaF_2 measured around $2\theta = 90°$ (8.5 on the y axis) on the SXD. Time of flight (on a logarithmic scale) is plotted against detector pixel in the equatorial plane of the detector. The centres of neighbouring pixels are about 1.2° apart in 2θ (*e.g.* pixel 5 corresponds to $2\theta = 85.8°$). The 220 Bragg peak occurs at about 6470 μs and the 440 at approximately 3235 μs.

Fig. 2 is a contour plot for the 16 different scattering angles in the equatorial plane around $2\theta = 90°$, showing the scattering in the region of the 220 and 440 reflections from a single crystal of barium fluoride. The sharp central peaks are the 220 and 440 Bragg reflections, which have largest intensities at the scattering angle $2\theta_B = 90°$. The TDS constitutes the remaining part of the pattern. The TDS occurs on one side only of each Bragg peak, where it rises to a pronounced maximum, the position of which changes from one scattering angle to the next. If t represents the time of flight for the TDS peak and t_B the time of flight for the Bragg peak, then the time difference $\Delta t = t - t_B$ increases progressively with the magnitude of the offset $\Delta 2\theta = 2\theta - 2\theta_B$ from the Bragg position. Fig. 3 is a plot of Δt *versus* $\Delta 2\theta$ for the 220 reflection. From this we find that the mean value of the ratio $(\Delta t / t_B)/\Delta 2\theta = 0.65$ (see below). As stated above, there is just one TDS peak recorded around the 440 reflection at each scattering angle for $2\theta_B = 90°$. The peak appears at shorter times of flight than the Bragg peak if $\Delta 2\theta < 0$ and at longer times if $\Delta 2\theta > 0$. On the other hand, for $2\theta_B = 125.5°$ there are two TDS peaks around the 440 reflection at a given scattering

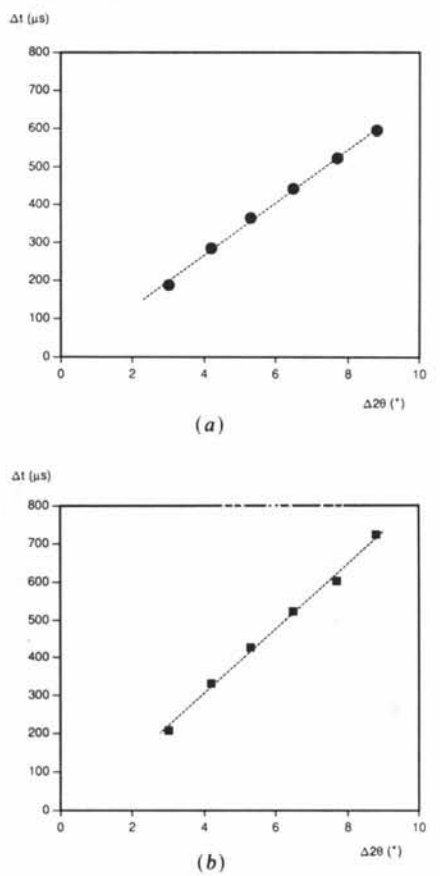

Fig. 3. Time displacement of the TDS peak from the Bragg position *versus* angle of offset for the 220 reflection: (*a*) phonon emission; (*b*) phonon absorption.

angle, as shown by the scattering pattern in Fig. 4. In this figure, one branch is due to phonon emission and the other to phonon absorption whereas, in Fig. 2, either the emission process or the absorption process takes place at a given scattering angle but not both.

These differences can be interpreted by recognizing that there are three regions of neutron velocity v_n to be considered in calculating the nature of the thermal diffuse scattering (Willis, 1986). If v_n exceeds the velocity of sound c_s in the crystal, the TDS rises to a maximum at the Bragg peak and scattering is allowed at all points in reciprocal space. If v_n lies between c_s and $c_s \cos\theta$, where θ is half the scattering angle, the TDS rises to a pair of maxima on either side of the Bragg peak and scattering between these maxima is forbidden. Finally, if v_n is less than $c_s \cos\theta$ there is only one maximum and this is associated with phonon emission for scattering angles less than the Bragg angle and with phonon absorption for scattering angles greater than the Bragg angle.

3. Theoretical interpretation

We define the one-phonon scattering surface as the locus in reciprocal space of the end points of the wave vectors that represent the scattered neutrons. For a crystal exhibiting isotropic propagation of sound, the scattering surface is a quadric surface, either a hyperboloid of two sheets or an ellipsoid (see Willis, 1986). This situation applies to barium fluoride for which the elastic anisotropy factor is close to unity (Carlile & Willis, 1989).

The condition for an ellipsoidal scattering surface is that

$$\beta \cos\theta > 1.$$

Here β is the ratio c_s/v_n, where c_s is the sound velocity and v_n the neutron velocity. There is then just one TDS peak. If β lies in the range

$$1 < \beta < \sec\theta,$$

the scattering surface is hyperboloidal and there are two TDS peaks. Clearly the first condition applies to the Bragg peaks shown in Fig. 2 and the 220 peak in Fig. 4 and the second to the 440 peak in Fig. 4.

We shall assume that the maximum intensity of the TDS peak in Fig. 2 corresponds to scattered radiation at the centre of the ellipsoidal scattering surface. It can then be shown (see Appendix) that the relation between Δt and $\Delta 2\theta$ is given by

$$\Delta t/\Delta 2\theta = \tfrac{1}{2} t_B (\tan\theta)/(\beta^2 \cos^2\theta - 1).$$

Using this formula with $\theta = 45°$ and inserting the average experimental value of 0.65 for $(\Delta t/t_B)/\Delta 2\theta$ gives a value of $\beta = 1.88$. The neutron velocity for Bragg scattering at $2\theta = 90°$ from the 220 planes is 1.28 km s^{-1}, so the measured velocity of sound is

$$c_s = \beta v_n = 2.40 \text{ km s}^{-1}.$$

This is close to the values 2.43 and 2.45 km s^{-1} that are measured for the hyperboloidal scattering surface, as observed in backscattering with the HRPD (Carlile & Willis, 1989).

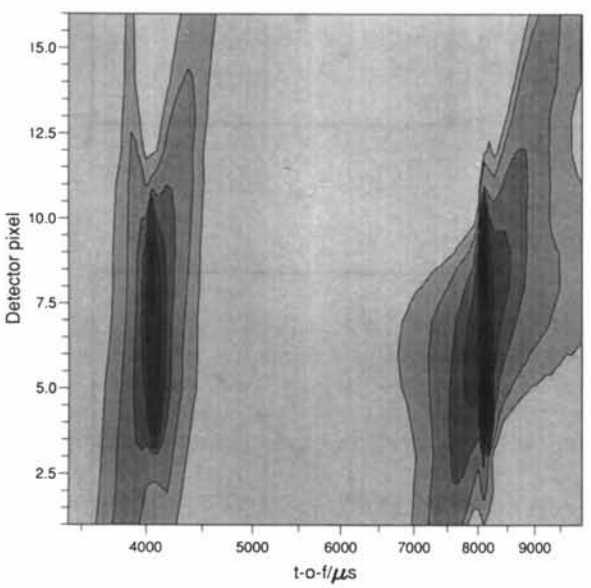

Fig. 4. Contour plot of the 220 and 440 reflections of BaF_2 measured around $2\theta = 125.5°$ on the SXD. The 220 Bragg peak occurs at about 8090 μs and the 440 at about 4045 μs. Note the appearance of two TDS peaks for each pixel value about the 440 Bragg peak.

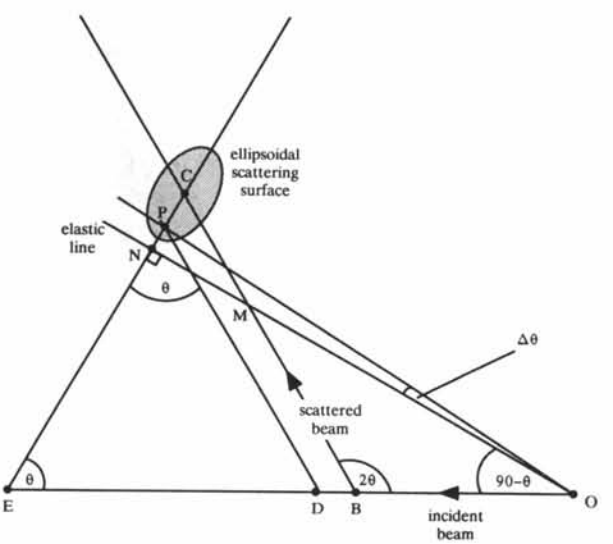

Fig. 5. The geometry of the one-phonon scattering process.

4. Concluding remarks

The nature of the thermal diffuse scattering in barium fluoride and calcium fluoride, as observed in time-of-flight neutron diffraction, was described earlier by Carlile & Willis (1989). These observations were restricted to the scattering régime in which the neutron velocity v_n was within the range

$$c_s > v_n > c_s \cos\theta,$$

where c_s is the velocity of sound in the crystal. For this régime there are two TDS peaks for a given offset angle from the Bragg position: one peak corresponds to phonon emisson and the other to phonon absorption.

In the present paper the measurements on barium fluoride have been extended to neutron velocities in the range

$$v_n < c_s \cos\theta.$$

Theory indicates that for this régime (Willis, 1986) there is only one TDS peak for a given offset angle $(\theta - \theta_B)$. The peak is due to phonon emisson for $\theta < \theta_B$ and to phonon absorption for $\theta > \theta_B$. Our measurements have confirmed the existence of this single peak and we have derived from it an estimate of the velocity of sound in BaF_2. This estimate is in good agreement with the independent value derived earlier from observations in the first velocity régime.

APPENDIX

To calculate the difference in time of flight between the TDS peak and the Bragg peak, we refer to the diagram in Fig. 5. Here O is the origin of reciprocal space, **OB** is the wave vector $\mathbf{k}_0$ of the incident beam and **BC** the wave vector of the scattered beam. The line ON at an angle $\pi/2-\theta$ to OB is the 'elastic line', *i.e.* the locus of the endpoints of scattered neutron wave vectors that undergo no change of energy on being scattered through 2θ. The centre of the ellipsoid scattering surface is represented by C; P is the nearest reciprocal-lattice point. P is at the focus of the ellipsoid and the elastic line ON coincides with the directrix.

From elementary geometry we have

$$CP = ae,$$

$$CN = a/e,$$

$$PN = a(1/e - e) = 2k_B(\sin\theta)\Delta\theta,$$

where $\mathbf{k}_B$ is the wave vector for Bragg scattering, $2a$ is the length of the major axis of the ellipsoid and e is its eccentricity. Also, OD in Fig. 5 has the length k_B, OB has length k_0, so

$$DB = k_B - k_0 = -\Delta k_0.$$

For the SXD, the path length of the scattered beam is much shorter than for the direct beam, so we can write

$$\Delta t/t_B = -\Delta k_0/k_B.$$

Recalling that $1/e = \beta\cos\theta$ (Willis, 1986), we obtain finally

$$\Delta t/\Delta 2\theta = \tfrac{1}{2}t_B(\tan\theta)/(\beta^2\cos^2\theta - 1).$$

References

CARLILE, C. J. & WILLIS, B. T. M. (1989). *Acta Cryst.* A**45**, 708-715.

SCHOFIELD, P. & WILLIS, B. T. M. (1987). *Acta Cryst.* A**43**, 803-809.

WILLIS, B. T. M. (1986). *Acta Cryst.* A**42**, 514-525.

WILLIS, B. T. M., CARLILE, C. J., WARD, R. C., DAVID, W. I. F. & JOHNSON, M. W. (1986). *Europhys. Lett.* **2**, 767-774.

Acta Cryst. (1992). A**48**, 829-834

A Note on the Darwin–Prins Rocking Curve for Perfect Crystals

BY NORIO KATO

Department of Physics, Faculty of Science and Engineering, Meijo University, Tenpaku-ku, Nagoya, Japan

(*Received* 3 *February* 1992; *accepted* 13 *April* 1992)

Abstract

For the purpose of calculating the reflectivity of perfect crystals in the Bragg case, taking into account both normal and Borrmann absorption, it is suggested that its original form is used expressed in terms of complex variables. Care is required regarding the phase angle for the algebraic expression of the square root. Two expressions which are directly usable for programming are presented. One of them is equivalent to the traditional one given by Zachariasen [*Theory of X-ray Diffraction in Crystals* (1945). New York: Wiley]. The other can be used without any problems of infinite values whatever values the

0108-7673/92/060829-06$06.00